https://doi.org/10.5194/amt-2019-236
Preprint. Discussion started: 9 August 2019

Atmospheric Measurement Techniques Discussions

An experimental study on light scattering matrices for Chinese loess dust with different particle size distributions

Jia Liu[1], Qixing Zhang[1], Jinjun Wang[1], Yongming Zhang[1]

[1]State Key Laboratory of Fire Science, University of Science and Technology of China, Hefei, Anhui, 230026, China

Correspondence to: Qixing Zhang (qixing@ustc.edu.cn) and Yongming Zhang (zhangym@ustc.edu.cn)

Abstract

Mineral dust suspended in the atmosphere has significant effects on radiative balance and climate change. Chinese Loess Plateau (CLP) is generally considered as a main sources of Asian dust aerosol. After being lifted by wind, dust particles with various size distributions can be transported for different distances. In this study, original loess sample was collected from Luochuan, which is centrally located at CLP, and two samples with different size distributions were obtained after then. "Pristine loess" was used to represent dust that only affect source regions, part of "pristine loess" was milled to finer "milled loess" that can be transported for long distance. Light scattering matrices for these two samples were measured at 532 nm wavelength from 5 ° to 160 ° angles. Particle size distribution, refractive index, chemical component, and microscopic appearance were also measured for auxiliary analyses. Results showed that discrepancies in angular behaviours of matrix elements for "pristine loess" and "milled loess" cannot be ignored. Given that the effective radii of these two loess samples differ by more than 20 times, it is reasonable to conclude that the difference in size distributions plays a major role in leading to different matrices, while refractive index and micro structure have relatively small impacts. Analyses of numerical simulation results about irregular particles also variety this conclusion. At last, synthetic scattering matrices for both "pristine loess" and "milled loess" were calculated over 0°-180 °, and the previous average scattering matrix for loess dust was updated.

1 Introduction

Mineral dust is a common particulate type in Earth's atmosphere, and accounts for a high fraction of atmospheric aerosol mass loading (Tegen and Fung, 1995). Asian dust contributes a lot to global atmospheric mineral dust load. Dust emitted from East Asia only is about 1.04×10^7 ton/year, 2.76×10^7 ton/year and 5.13×10^7 ton/year for PM_{10} (particles with aerodynamic equivalent diameter smaller than 10μm), PM_{30} and PM_{50} (Xuan et al., 2004). During aerosol characterization experiments (ACE-Asia), mass balance calculations indicated that 45-82 % of the observed total aerosol mass can be attributed to Asian dust (Zhang et al., 2003). Chinese Loess Plateau (CLP) is usually considered as a main sources or an important supply site of Asian dust aerosol (Han et al., 2008; Shen et al., 2016; Tsai et al., 2014; Zhang et al., 2010). Statistical analysis of dust storms influencing Chinese Mainland from 2000 to 2002 showed that about a quarter of dust

https://doi.org/10.5194/amt-2019-236
Preprint. Discussion started: 9 August 2019


Atmospheric Measurement Techniques Discussions

storms were originated from CLP (Zhang and Gao, 2007). Source tracing of dust collected in Xi'an revealed that these dust particles were mainly short-distance transported from CLP (Yan et al., 2015). Comparison of chemical element ratios demonstrated that dust particles emitted from CLP can be transported to Korea, Japan and North Pacific (Cao et al., 2008).

Because of the scattering and the absorption of solar radiation, atmospheric dust can have remarkable influences on global climate change as well as radiation budget (Satheesh and Moorthy, 2005; Sokolik and Toon, 1996). It is common knowledge that dust particles with different sizes can be transported to different distances. Dust particles with a size range of $r > 5$ μm exist in source areas only, while particles with a size range of $0.1 < r < 5$ μm can experience airborne transportation over long distances (like about 5000 km), even cross-continent from Asia to North America (Jaffe et al., 1999; Satheesh and Moorthy, 2005). Therefore, loess dust emitted from CLP will have important influence on the radiation balance at both source areas and places far away from sources. Characterizations of optical properties and other basic physical features of loess dust with different sizes are beneficial to obtain better understandings of remote sensing observations and radiative forcing effects of loess dust at source region and after long-range transportation.

Without any doubt, optical properties of dust particles vary with changes of their size distributions. Light scattering matrix $\boldsymbol{F}$, a 4×4 matrix containing 16 elements F_{ij} (i, j=1-4), is a fundamental optical property that can be used to characterize airborne dust particulates (Volten et al., 2001). Scattering matrix is not only sensitive to size distribution but also sensitive to other physical features like particle shape, micro structure and refractive index (Muñoz and Hovenier, 2011). Therefore, it can be employed as a useful parameter to give information and implication about above features of dust particles. Based on similar operational principles, several light scattering matrix measurement apparatus were developed by researchers in the past two decades (Liu et al., 2018; Muñoz et al., 2010; Volten et al., 2001; Wang et al., 2015). With the assistant of these apparatus, scattering matrices for various mineral dust were experimentally determined, such as loess, clay, desert dust, volcanic ash, simulant of cosmic dust and so on (Dabrowska et al., 2015; Escobar-Cerezo et al., 2018; Merikallio et al., 2015; Muñoz et al., 2007; Muñoz et al., 2001). In addition, Amsterdam Database and Amsterdam-Granada Database were established at 2005 and 2012 to publish measured scattering matrices as well as necessary physical properties of mineral dust particles (Volten et al., 2005; Volten et al., 2006a; Muñoz et al., 2012).

Most published literatures of experimental measurements of scattering matrices focused more on similarities and discrepancies between different kinds of mineral dust, or between the same kinds of dust sampled from different sources. Furthermore, there are still some researches pay attention to the effect of particle size distribution on scattering matrices. Olivine dust with four size distributions were obtained using different sieves, but there are no clear and consistent effects of size on measured scattering matrices for olivine at both 442 nm and 633 nm wavelengths (Muñoz et al., 2000). Forsterite samples were produced with three size distributions using dry and wet sieving method, comparisons of experimental scattering matrices at 632.8 nm wavelength clearly showed the influence of size (Volten et al., 2006b). Relative phase function is larger for large forsterite particles, F_{22}/F_{11} is larger for small particles, $-F_{12}/F_{11}$ and F_{34}/F_{11} for small particles are larger at most scattering angles but there are opposite trend for the negative branches at backscattering angles, F_{33}/F_{11} and F_{44}/F_{11} for small particles are larger at forward scattering angles while are smaller at backscattering angles. Two samples of

https://doi.org/10.5194/amt-2019-236
Preprint. Discussion started: 9 August 2019


Atmospheric Measurement Techniques Discussions

palagonite with different size distributions were prepared by heating, analyses of measured $-F_{12}/F_{11}$ revealed that small particles have larger $-F_{12}/F_{11}$ values at both 488 nm and 647 nm wavelengths (Dabrowska et al., 2015). Three commercial samples of Arizona Road Dust with ultrafine, fine and medium particles were selected to investigate their scattering matrices, results demonstrated that ultrafine particle has the largest normalized phase function while medium particle has the smallest F_{22}/F_{11} (Wang et al., 2015). Lunar soil simulant JSC-1A particles were recovered and reused during scattering matrices measurement experiments, and recovered sample was larger than pristine sample. Comparative analyses indicated that large particles have larger relative phase function and $-F_{12}/F_{11}$, large particles have smaller F_{22}/F_{11} at forward scattering angles while F_{22}/F_{11} for these two samples were consistent at backscattering angles (Escobar-Cerezo et al., 2018). Experimentally determined $-F_{12}/F_{11}$ for meteorites illustrated that the minimum value of $-F_{12}/F_{11}$ for larger particles is smaller, and the maximum value of $-F_{12}/F_{11}$ for larger particles is larger (Frattin et al., 2019).

It can be concluded from above researches that size distributions have inconsistent effects on scattering matrix elements for various dust particles. And there is no study pay attention to the effect of size distribution on scattering matrix for loess dust. Therefore, original loess sample was collected from rural areas of Luochuan, the center of CLP, in this research. After sieving to remove large particles, "pristine loess" sample was used to represent loess dust that is only present in source regions. Furthermore, part of "pristine loess" was ball-milled to obtain finer "milled loess" sample that can be transported for long distance and affect regions far away from dust sources. Scattering matrices for above loess samples with distinct size distributions were measured at 532 nm with the help of a self-developed apparatus over angles 5 °-160 °. Besides particle size distribution, other characteristics that might be changed during milling process were also analyzed, such as chemical component, refractive index and microscopic appearance. Discrepancies in angular behaviors of matrix elements and their reasons were analyzed. Furthermore, synthetic scattering matrices were defined over 0 °-180 °, and the previously published average scattering matrix for loess was updated.

In Section 2, fundamental characteristics of "pristine loess" and "milled loess" samples are shown. In Section 3, concise introduction of related theory, apparatus and methods are given. In Section 4, measured and synthetic scattering matrices for these two samples are plotted, reasons leading to these discrepancies in matrix elements are discussed and previous average scattering matrix for loess is updated. At last, in Section 5, conclusions are drawn.

2 Fundamental Characteristics of Loess Dust Samples

There are two deserts in the northern of Chinese Loess Plateau, and according to the distances from these deserts, CLP is roughly separated into 3 regions: sandy loess, loess as well as clayey loess (Cao et al., 2008). Original loess dust sample was collected from Loess National Geological Park (35.76°N, 109.42°E) at Luochuan, lying on the "loess zone" and also at the center of CLP. Therefore, it can be considered that the sample collected is the most representative of loess of China. Prior to laboratory researches, large particles in original sample were removed through a 50 μm sieve. Next, the original loess sample was divided into two parts, one of which was not treated any more and was called as "pristine loess", and the other

https://doi.org/10.5194/amt-2019-236
Preprint. Discussion started: 9 August 2019

Atmospheric Measurement Techniques Discussions

was milled by a ball miller to obtain finer particles, called as “milled loess”. It should be noted that "milled loess" is the same sample as the "Luochuan loess" in reference (Liu et al., 2019). Both of these two loess dust samples were investigated in light scattering matrices measurements as well as other auxiliary analyses of physical characteristics of particles.

The size distributions of “pristine loess” and “milled loess” were determined by a laser particle sizer (SALD-2300; Shimadzu), three independent repeated measurements were conducted for each sample. As can be seen from Figure 1, the size of “pristine loess” shows a distinct bimodal distribution, after ball milling, particle size of “milled loess” becomes a unimodal distribution and the distribution is more concentrated. From the viewpoint of atmospheric particle transportation, the majority (more than 70%) of “pristine loess” particles have radii larger than 5 μm, thus this sample can be used to represent coarse dust that only affect source region, like Xi’an City (Yan et al., 2015). On the other hand, almost all particles of “milled loess” sample have radii smaller than 2 μm, and can be used to as a representative of fine loess dust that can be transported for long distance and affect regions far away from dust sources. Using light intensity distribution reproduction method, appropriate refractive indices m for measured samples can be calculated automatically by the size analyzer. During size distribution measurements of loess samples, this method was employed, with the retrieval ranges of real part $Re(m)$ and imaginary part $Im(m)$ of refractive index preset as 1.45-1.75 and 0-0.05, respectively (Volten et al., 2001). As shown in Table 1, the optimal refractive indices are $1.65+0i$ for “pristine loess” and $1.70+0i$ for “milled loess”, larger particles have relatively larger real part of refractive index. Using measured result, effective radius r_{eff} as well as standard deviation σ_{eff} can be derived (Hansen and Travis, 1974):

$$r_{eff} = \frac{\int_0^\infty r\pi r^2 n(r)dr}{\int_0^\infty \pi r^2 n(r)dr} \quad (1)$$

$$\sigma_{eff} = \sqrt{\frac{\int_0^\infty (r-r_{eff})^2 \pi r^2 n(r)dr}{r_{eff}^2 \int_0^\infty \pi r^2 n(r)dr}} \quad (2)$$

where $n(r)dr$ stands for number proportion of equivalent spheres whose radii vary between r and $r+dr$. Results of r_{eff} and σ_{eff} are shown in Table 1. In addition, effective size parameters $x_{eff} = 2\pi r_{eff}/\lambda$ for “pristine loess” and “milled loess” were also calculated and are presented in Table 1.

Figure 1

Table 1

Scanning electron microscope (SEM) photographs for “pristine loess” (left panel) and “milled loess” (right panel) are displayed in Figure 2. Obviously, particles of these two samples exhibit various shapes, and all of the particles can be classified as irregular shape. Almost all particles have rough surfaces and some particles even have sharp edges. After the milling process, there are more sub-micron particles in “milled loess” sample, some small particles even stuck on the rough surface of large particles due to electrostatic forces.

Figure 2

https://doi.org/10.5194/amt-2019-236
Preprint. Discussion started: 9 August 2019

Atmospheric Measurement Techniques Discussions

During the milling process, commercially man-made ZrO_2 grinding balls were used. For the purpose of detecting whether the chemical compositions of loess samples were changed, the oxide compositions of samples before and after milling process, that is the "pristine loess" and "milled loess", were determined using a X-ray fluorescence spectrometer (XRF-1800, Shimadzu). As can be seen from Table 2, the difference in the content of ZrO_2 between these two loess samples is small, indicating that the wear of ZrO_2 balls during grinding process is negligible. The largest variation of content occurs for SiO_2, but this variation is less than 2%. Thus it can be concluded that milling process has little effect on chemical compositions for loess samples.

Table 2

3 Theoretical Background and Experimental Methodology

3.1 Basic Concepts about Light Scattering Matrix

Four Stokes parameters (*I*, *Q*, *U* and *V*) are usually used to introduce the intensity and polarization properties of light beam. And these parameters can form a column vector, the so called Stokes vectors (Hovenier et al., 2014; Hulst and Van De Hulst, 1981). If a cloud of particles present in light path, the incident beam will be scattered and part of light will deviate from the original direction of propagation. When multi-scattering only plays a negligible role, intensity and polarization state for scattered beams can be calculated from that of incident beam, using a 4×4 light scattering matrix $\boldsymbol{F}$ (Mishchenko and Yurkin, 2017):

$$\begin{pmatrix} I_{sca} \\ Q_{sca} \\ U_{sca} \\ V_{sca} \end{pmatrix} = \frac{\lambda^2}{4\pi^2 D^2} \begin{pmatrix} F_{11}(\theta) & F_{12}(\theta) & F_{13}(\theta) & F_{14}(\theta) \\ F_{21}(\theta) & F_{22}(\theta) & F_{23}(\theta) & F_{24}(\theta) \\ F_{31}(\theta) & F_{32}(\theta) & F_{33}(\theta) & F_{34}(\theta) \\ F_{41}(\theta) & F_{42}(\theta) & F_{43}(\theta) & F_{44}(\theta) \end{pmatrix} \begin{pmatrix} I_{inc} \\ Q_{inc} \\ U_{inc} \\ V_{inc} \end{pmatrix} \quad (3)$$

where λ stands for wavelength of light, *D* is the distances between particle cloud and light detectors, scattering angle θ is the angle between incident and scattered beams, and the scattering plane contains both incident and scattered beams.

Generally, $\boldsymbol{F}$ has 16 independent matrix elements F_{ij} with *i*, *j*=1-4. And two basic assumptions are commonly used to simplify the general form of light scattering matrix. The first one is that all scattering planes are equivalent for particles having random orientations. Thus, scattering directions can be adequately depicted by θ. The second one is that particles and their mirror counterparts exist in the same number in a cloud of randomly oriented particles. Based on the above randomly orientation and mirror particle assumptions the number of independent elements in light scattering matrix can be reduced from 16 to 6 (Mishchenko and Yurkin, 2017):

$$\boldsymbol{F} = \begin{pmatrix} F_{11}(\theta) & F_{12}(\theta) & 0 & 0 \\ F_{12}(\theta) & F_{22}(\theta) & 0 & 0 \\ 0 & 0 & F_{33}(\theta) & F_{34}(\theta) \\ 0 & 0 & -F_{34}(\theta) & F_{44}(\theta) \end{pmatrix} \quad (4)$$

https://doi.org/10.5194/amt-2019-236
Preprint. Discussion started: 9 August 2019

Atmospheric Measurement Techniques Discussions

3.2 Experimental Apparatus and Methodology

Figure 3 shows a picture of scattering matrix measurement apparatus. The wavelength of incident beam is 532 nm, and there are a linear polarizer *P* as well as an electro-optic modulator *EOM* in its propagation path. Subsequently, the modulated incident light is scattered by dust aerosols produced using an aerosol generator. A photomultiplier *Detector* is encapsulated in a dark cassette along with a 532 nm quarter-wave plate *Q* as well as a polarizer *A*. Before the scattered light is detected by the Detector, it successively passes through *Q* and *A*. The cassette is fixed on a rotation arm, rotation center of which coincides with the center of aerosol nozzle. *Detector* is controlled by a motor and is able to scan scattering angles from 5 ° to 160 °. Another photomultiplier *Monitor* is fixed at 30 °scattering angle to record variations of dust aerosols. The combination of electro-optic modulator and lock-in detector allows multiple scattering matrix elements or their sums can be measured simultaneously. All the matrix elements of dust samples can be determined as functions of scattering angles with the help of various combinations of orientation angles of above optical elements (Muñoz et al., 2010). Fluctuations of dust aerosols can be eliminated by normalizing *Detector* measurements through *Monitor* measurements. The optical platform is surrounded by black curtains to avoid the effect of environmental stray light. Furthermore, background signals need to be measured and subtracted. Subsequently, $F_{11}(\theta)$ is normalized to 1 at 10 ° scattering angle, and remaining matrix elements $F_{ij}(\theta)$ are normalized to $F_{11}(\theta)$ at the same angle. At last, whether measurement results of scattering matrix satisfy Cloude coherency matrix test should be examined (Hovenier and Van Der Mee, 1996). For more details, it can be referred to Muñoz et al. (2010) and Liu et al. (2018).

Figure 3

A dust generator (RBG 1000; Palas) was applied to disperse loess particles (Liu et al., 2018). Dust particles were transmitted to scattering zone by airstream and some particles in each loess sample were sprayed to different vessels for subsequent size analyses. For reliable measurement results, experiments should be conducted under single scattering conditions. This requires that the number of particles in the scattering body be appropriate, too many particles will cause significant multiple scattering, while too few particles will cause the two basic assumptions mentioned above to be dissatisfied. Incident light intensity I_0 as well as transmitted light intensity I passing through a cloud of particles can be related by the following equation (Mokhtari et al., 2005):

$$I = I_0 e^{-\langle s \rangle} \tag{5}$$

where <s> stands for average number of scattering events. P(2)/P(1)=<s>/2 is used to describe the ratio of occurrence probability of double scattering event (the simplest form of multi-scattering) to that of single scattering event (Wang et al., 2015).

https://doi.org/10.5194/amt-2019-236
Preprint. Discussion started: 9 August 2019

Atmospheric Measurement Techniques Discussions

4 Results and Discussions

4.1 Experimentally Determined Scattering Matrices

The measurements of <s>/2 were conducted before the measurements of matrix elements using each orientation angle combination of above optical elements. Measured <s>/2 for both "pristine loess" and "milled loess" were smaller than about 0.006, in other word, the occurrence probability of double scattering event was about 170 times smaller than that of single scattering event and double scattering event can be ignored without question. For each loess sample, three independent and replicated measurements were conducted, and the experimental results shown in figures are averaged values for three measurements. And examinations showed that measurements of loess samples satisfy Cloude coherency matrix test at all scanned scattering angles.

Experimentally determined scattering matrix elements for both "pristine loess" and "milled loess" are shown in Figure 4. Ratios $F_{13}(\theta)/F_{11}(\theta)$, $F_{14}(\theta)/F_{11}(\theta)$, $F_{23}(\theta)/F_{11}(\theta)$, and $F_{24}(\theta)/F_{11}(\theta)$ are not plotted, because these ratios do not deviate from zero within experimental errors. Matrix elements for "pristine loess" and "milled loess" samples present similar angular behaviors and all six non-zero matrix elements are limited to narrow regions, respectively. Normalized phase functions $F_{11}(\theta)/F_{11}(10°)$ show strong forward scattering peaks, variations at backscattering directions are not obvious, which are typical behaviors for mineral dust with irregular shapes (Muñoz et al., 2012; Volten et al., 2001). For non-polarized incident beam, $-F_{12}(\theta)/F_{11}(\theta)$ is equivalent to the degree of linear polarization. Measured angular behaviors of $-F_{12}(\theta)/F_{11}(\theta)$ are bell-shaped, and their largest values appear at near side-scattering directions. There are negative branches of $-F_{12}(\theta)/F_{11}(\theta)$ at forward scattering directions, and according to Dabrowska et al. (2015), other negative branches are likely to appear at backscattering directions. $F_{22}(\theta)/F_{11}(\theta)$ is a proof of the non-sphericity and irregularity of particles, since it is constant 1 for homogeneous spheres. Measured values of these two loess samples show that $F_{22}(\theta)/F_{11}(\theta)$ ratios deviate from constant 1 at nearly all angles scanned. The ratios $F_{33}(\theta)/F_{11}(\theta)$ and $F_{44}(\theta)/F_{11}(\theta)$ can be studied jointly because these two ratios are equal for particles with spherical shape. But for loess dust, $F_{33}(\theta)/F_{11}(\theta)$ values are smaller than $F_{44}(\theta)/F_{11}(\theta)$, especially at backscattering directions. The ratios $F_{34}(\theta)/F_{11}(\theta)$ show "S-type" shapes and maximums are obtained at near 110° angles. When scattering angles are less than 50°, the values of $F_{34}(\theta)/F_{11}(\theta)$ are negative.

Figure 4

However, the discrepancies in matrix elements for "pristine loess" and "milled loess" cannot be ignored. Compared to "milled loess", it can be observed an increase of relative phase function at 5° scattering angle for "pristine loess". Relative phase function for "pristine loess" is also larger at side and back scattering angles. As for ratio $-F_{12}(\theta)/F_{11}(\theta)$, smaller "milled loess" sample has smaller maximum values at near side scattering angles, while larger "pristine loess" has relatively larger values. Different from ratio $-F_{12}(\theta)/F_{11}(\theta)$, measured $F_{34}(\theta)/F_{11}(\theta)$ is larger for smaller "milled loess" sample. Experimentally determined $F_{22}(\theta)/F_{11}(\theta)$ values of "milled loess" are larger than "pristine loess", especially at side and back scattering angles. As for ratios $F_{33}(\theta)/F_{11}(\theta)$ and $F_{44}(\theta)/F_{11}(\theta)$, the measurements for "milled loess" are larger than the values for "pristine loess".

https://doi.org/10.5194/amt-2019-236
Preprint. Discussion started: 9 August 2019


Atmospheric Measurement Techniques Discussions

In this study, several fundamental characteristics of loess dust samples were measured for auxiliary analyses, including size distribution, refractive index, chemical component and microscopic appearance. As shown in Table 1, effective radii for "pristine loess" and "milled loess" are 49.40 and 2.35, respectively. The real part of refractive index for "pristine loess" is 1.65 and that for "milled loess" is 1.70. Table 2 shows that the largest change of chemical content (SiO_2) is less than 2%. Furthermore, it can be seen from Figure 2 that loess dust become more irregular after milling process, because small particles attached on the surface of large particle. Among all these characteristics, particle effective radii for "pristine loess" and "milled loess" differ by more than 20 times, and this can be thought as the biggest difference between the two samples. Therefore, it is reasonable to conclude that above differences in angular distributions of scattering matrix elements may be mainly caused by different size distributions. While other factors such as refractive index and micro structure have relatively small impact.

In this work, several literatures about optical modeling of irregular mineral dust were analyzed to find reasonable explanations of the differences in scattering matrix elements for "milled loess" and "pristine loess" samples. Numerical simulations of Gaussian spheres show that as effective radius increases from 30 to 600, phase function F_{11} as well as ratios F_{33}/F_{11} and F_{44}/F_{11} decrease, the maximum of ratio F_{34}/F_{11} decreases and negative branches at forward scattering and backscattering directions disappear, the maximum of ratio $-F_{12}/F_{11}$ increases, and the ratio F_{22}/F_{11} increase especially at back scattering angles (Liu et al., 2015). When Gaussian spheres become more non-spherical and irregular, phase function F_{11} as well as ratios $-F_{12}/F_{11}$, F_{22}/F_{11}, F_{33}/F_{11} and F_{44}/F_{11} show different trends compared with the influence of increasing effective radius, while the ratios F_{34}/F_{11} show similar trend (Liu et al., 2015). Zubko et al. (2007) showed that as the surfaces of Gaussian particles become rougher, the ratio $-F_{12}/F_{11}$ tends to larger. Simulations of agglomerated debris particles showed that with the imaginary part of refractive index varies in the range 0-0.01, scattering matrix elements almost unchanged (Zubko et al., 2013). Calculations of Gaussian particles conducted by Muinonen et al. (2007) showed that the increase of refractive index (both real and imaginary part) leads to smaller $-F_{12}/F_{11}$ and F_{22}/F_{11}. In summary, it seems that the discrepancies between "milled loess" and "pristine loess" can be interpreted from the point of difference of effective radii, with the help of simulation result of Gaussian spheres. However, different factors have different or similar effects on a certain matrix elements. Factors such as refractive index and micro structure may also contribute to the final angular distributions of scattering matrices. Thus, it is concluded that difference of size distribution plays the major role, while other factors are also not ignorable.

Since particles with different sizes can be transported for different distances, affecting radiation balance in various regions. Thus, it is important to explore the effects of size distributions on scattering matrices for different kinds of dust samples through laboratory measurements. In this work, a relatively good case is presented to show the effect of size distribution of loess dust on scattering matrices because effective radii of "pristine loess" and "milled loess" differ by more than 20 times. And the influence of loess particle size can be verified by the simulation results of the Gaussian sphere, which deepen the understanding of this effect. However, as discussed above, besides size distribution, physical properties such as refractive index and micro structure also play important roles in determining scattering matrices of dust samples. When the

https://doi.org/10.5194/amt-2019-236
Preprint. Discussion started: 9 August 2019

Atmospheric Measurement Techniques Discussions

relative difference in particle size distributions or effective radii is small, the influences of other factors may become dominant or un-ignorable. This may be the reason why the effect of size distributions on measured scattering matrices for olivine samples cannot be concluded clearly (Muñoz et al., 2000). And this may also be the reason why effective radii cannot be used to explain all the discrepancies in matrix elements for forsterite samples according to simulation results of Gaussian spheres (Volten et al., 2006b). In addition, another reason may be that Gaussian spheres are not suitable models to reproduce scattering matrix for forsterite dust, as optical modelling of irregular mineral dust is a challenging subject.

4.2 Synthetic Scattering Matrices

Laboratory measurements of scattering matrices only cover scattering angle from 5 ° to 160 °. In order to obtain scattering matrix over 0 °-180 °, synthetic scattering matrices $\boldsymbol{F}^{syn}$ are constructed by a combination of numerical simulation and extrapolation or interpolation of experimental measurements (Dabrowska et al., 2015; Escobar-Cerezo et al., 2018).

Measured $F_{11}(\theta)$ values are normalized to 1 at 10 °, and these relative phase functions are the same for measured and synthetic scattering matrix of the same sample (Escobar-Cerezo et al., 2018):

$$\frac{F_{11}(\theta)}{F_{11}(10°)} = \frac{F_{11}^{syn}(\theta)}{F_{11}^{syn}(10°)} \quad (6)$$

where $F_{11}^{syn}(\theta)$ is the synthetic phase function that must fulfill the following normalized equation:

$$\frac{1}{2}\int_0^{\pi} d\theta sin\theta F_{11}^{syn}(\theta) = 1 \quad (7)$$

SEM images for both loess samples show that most particles have relatively moderate aspect ratios. Therefore, Lorenz-Mie theory can be used for calculations of forward peaks of synthetic phase function at angles smaller than 5 °. Because for particles who have moderate aspect ratios, forward peaks of synthetic phase functions mainly depend on size distributions and depend little on particle shape (Liu et al., 2003). Refractive indices as well as size distributions of “pristine loess” and “milled loess” obtained from particle sizer were used in Lorenz-Mie calculations. For scattering angles from 160 °to 180 °, 9-order polynomial extrapolation is used on the basis of experimentally determined relative phase functions. After then, the calculated forward peak of phase function as well as relative phase function after extrapolated are incorporated at 5 °angle to construct synthetic phase function. Whether synthetic phase function satisfies Eq. (7) should be checked. Otherwise, increase or decrease measured relative phase function at 5 °angle within measurement error, and repeat merging process and checking process until Eq. (7) is satisfied.

As for other matrix element ratios $F_{ij}(\theta)/F_{11}(\theta)$, a set of constraints at 0 °and 180 °scattering angles should be taken into consideration (Hovenier et al., 2014; Mishchenko and Hovenier, 1995):

$$\frac{F_{12}(0°)}{F_{11}(0°)} = \frac{F_{12}(180°)}{F_{11}(180°)} = \frac{F_{34}(0°)}{F_{11}(0°)} = \frac{F_{34}(180°)}{F_{11}(180°)} = 0 \quad (8)$$

$$\frac{F_{22}(0°)}{F_{11}(0°)} = \frac{F_{33}(180°)}{F_{11}(180°)} = 1 \quad (9)$$

https://doi.org/10.5194/amt-2019-236
Preprint. Discussion started: 9 August 2019

Atmospheric Measurement Techniques Discussions

$$\frac{F_{22}(180°)}{F_{11}(180°)} = -\frac{F_{33}(180°)}{F_{11}(180°)} \quad (10)$$

$$\frac{F_{44}(180°)}{F_{11}(180°)} = 1 - 2\frac{F_{22}(180°)}{F_{11}(180°)} \quad (11)$$

Synthetic values for ratio F_{22}/F_{11} at angles from 160° to 180° for "pristine loess" and "milled loess" are obtained by five-order polynomial extrapolations. Then F_{33}/F_{11} and F_{44}/F_{11} at 180 ° are calculated according to Eqs. (10) and (11), respectively, and values of these two ratios at remaining angles are obtained by cubic spline interpolation. Values of ratios F_{12}/F_{11} and F_{34}/F_{11} at missing angles are also obtained using cubic spline interpolation. In addition, right-hand (left-hand) derivative at 0 ° (180 °) for each scattering matrix element must be 0 (Hovenier and Guirado, 2014). In Figure 5, these synthetic matrices for "pristine loess" and "milled loess" are illustrated.

Figure 5

Using extrapolated value of F_{22}/F_{11} at 180 ° scattering angle, back-scattering depolarization ratio δ_L can be calculated, which is an essential parameter for lidar observations (Mishchenko et al., 2002):

$$\delta_L = \frac{F_{11}(180°) - F_{22}(180°)}{F_{11}(180°) + F_{22}(180°)} = \frac{1 - \frac{F_{22}(180°)}{F_{11}(180°)}}{1 + \frac{F_{22}(180°)}{F_{11}(180°)}} \quad (12)$$

Calculated back-scattering depolarization ratios for "pristine loess" and "milled loess" are 0.203 and 0.256, respectively, "milled loess" has larger value of δ_L. Direct measurements of back-scattering depolarization ratios of Arizona Test Dust with different size distributions at both 355 and 532 nm wavelengths also showed that δ_L values for small particles are larger than that for large particles and this discrepancy is more pronounced at 532 nm (Miffre et al., 2016).

At last, the previously presented average scattering matrix for loess was updated with new sample "pristine loess" included, by averaging synthetic matrices for different loess samples. As shown in Figure 6, after average synthetic scattering matrix being updated, new phase function becomes larger at forward peak and smaller at side- and back-scattering angles, ratio $-F_{12}(\theta)/F_{11}(\theta)$ increases at side-scattering directions and covers more domain, ratio $F_{22}(\theta)/F_{11}(\theta)$ experiences the largest change with values at nearly all scattering angles tend to larger, and ratios $F_{33}(\theta)/F_{11}(\theta)$ and $F_{44}(\theta)/F_{11}(\theta)$ become smaller at near backscattering directions and cover more areas.

Figure 6

5 Conclusions

Asian dust contributes a lot to global atmospheric dust aerosol, and Chinese Loess Plateau (CLP) is a main origin of Asian dust. Loess dust aerosols originated from CLP will affect the radiation balance potentially at both source areas and places far away from sources, because dust particles with different sizes can be transported to different distances. In this study, original loess sample was collected from rural areas of Luochuan, which is centrally located at CLP. Subsequently, two loess samples with different size distributions were prepared for laboratory investigations. "Pristine loess" sample was

https://doi.org/10.5194/amt-2019-236
Preprint. Discussion started: 9 August 2019


Atmospheric Measurement Techniques Discussions

used to represent loess dust that affect source regions only. And "milled loess" sample ball-milled from "pristine loess" was used to represent loess dust that can be transported for long distance. Light scattering matrices for both "pristine loess" and "milled loess" samples at 532 nm wavelength were measured, from 5° to 160°scattering angles. Besides particle size distribution, other basic characteristics were also measured, such as chemical component, refractive index and microscopic appearance.

The angular behaviors of scattering matrix elements for "pristine loess" and "milled loess" present significant similarity, just like all other kinds of mineral dust with irregular shape. However, the discrepancies in matrix elements still cannot be ignored. For small "milled loess", relative phase function $F_{11}(\theta)/ F_{11}(10°)$ is smaller, ratios $F_{33}(\theta)/F_{11}(\theta)$, $F_{34}(\theta)/F_{11}(\theta)$ and $F_{44}(\theta)/F_{11}(\theta)$ are larger, while ratios $-F_{12}(\theta)/F_{11}(\theta)$ and $F_{22}(\theta)/F_{11}(\theta)$ are smaller. These differences can be results of comprehensive effect of changes of size distribution, refractive index and particle micro structure caused by milling process. Given that effective radius of these two loess samples differ by more than 20 times, so it is reasonable to conclude that the difference of size distributions plays a major role in leading to different matrices, other factors such as refractive index and micro structure have relatively small impacts. Analyses of numerical simulation results about irregular particles also verify this conclusion. Synthetic scattering matrices for both "pristine loess" and "milled loess" were defined over 0°-180° scattering angle range, which will facilitate the application of measurements in radiative transfer calculation. And the previously presented average scattering matrix for loess was updated with new sample "pristine loess" included.

Data availability

All the data involved in this study are available upon request to the corresponding authors.

Author contributions

Jia Liu and Qixing Zhang designed the experiments; Jia Liu conducted the measurements; all authors discussed the results; Jia Liu wrote the manuscript.

Competing interests

The authors declare that they have no conflict of interest.

Acknowledgements

We are very grateful to Zidong Nie for loess dust sampling. We are also very grateful to Engineer Chao Li from HEFEI KE JING MATERIALS TECHNOLOGY CO., LTD. for milling dust particles. This work was financially supported by the National Natural Science Foundation of China (NSFC) (41675024 and U1733126), National Key Research and

https://doi.org/10.5194/amt-2019-236
Preprint. Discussion started: 9 August 2019

Atmospheric Measurement Techniques Discussions

Development Program of China (2016YFC0800100 and 2017YFC0805100], and Fundamental Research Funds for Central Universities of China (WK2320000035).

References

Cao, J., Chow, J., Watson, J., Wu, F., Han, Y., Jin, Z., Shen, Z., and An, Z.: Size-differentiated source profiles for fugitive dust in the Chinese Loess Plateau, Atmospheric Environment, 42(10), 2261-2275, doi:10.1016/j.atmosenv.2007.12.041, 2008.

Dabrowska, D. D., Muñoz, O., Moreno, F., Ramos, J. L., Martínez-Frías, J., and Wurm, G.: Scattering matrices of Martian dust analogs at 488 nm and 647 nm, Icarus, 250, 83-94, https://doi.org/10.1016/j.icarus.2014.11.024, 2015.

Escobar-Cerezo, J., Muñoz, O., Moreno, F., Guirado, D., Gómez Martín, J., Goguen, J., Garboczi, E., Chiaramonti, A., Lafarge, T., and West, R.: An Experimental Scattering Matrix for Lunar Regolith Simulant JSC-1A at Visible Wavelengths, The Astrophysical Journal Supplement Series, 235(1), 19, https://doi.org/10.3847/1538-4365/aaa6cc, 2018.

Frattin, E., Muñoz, O., Moreno, F., Nava, J., Escobar-Cerezo, J., Gomez Martin, J., Guirado, D., Cellino, A., Coll, P., Raulin, F., Bertini, I., Cremonese, G., Lazzarin, M., Naletto, G. and La Forgia, F.: Experimental phase function and degree of linear polarization of cometary dust analogues, Monthly Notices of the Royal Astronomical Society, 484(2), 2198-2211, https://doi.org/10.1093/mnras/stz129, 2019.

Han, Y., Cao, J., Posmentier, E. S., Fung, K., Tian, H., and An, Z.: Particulate-associated potentially harmful elements in urban road dusts in Xi'an, China, Applied Geochemistry, 23(4), 835-845, doi:10.1016/j.apgeochem.2007.09.008, 2008.

Hansen, J. E., and Travis, L. D.: Light scattering in planetary atmospheres, Space science reviews, 16(4), 527-610, https://doi.org/10.1007/BF00168069, 1974.

Hovenier, J., and Guirado, D.: Zero slopes of the scattering function and scattering matrix for strict forward and backward scattering by mirror symmetric collections of randomly oriented particles, Journal of Quantitative Spectroscopy and Radiative Transfer, 133, 596-602, https://doi.org/10.1016/j.jqsrt.2013.09.023, 2014.

Hovenier, J., and Van der Mee, C.: Testing scattering matrices: a compendium of recipes, Journal of Quantitative Spectroscopy and Radiative Transfer, 55(5), 649-661, https://doi.org/10.1016/0022-4073 (96)00008-8, 1996.

Hovenier, J. W., Van der Mee, C. V., and Domke, H.: Transfer of polarized light in planetary atmospheres: basic concepts and practical methods, Berlin/Heidelberg, Germany, Springer Science & Business Media, 2014.

Hulst, H. C., and van de Hulst, H. C.: Light scattering by small particles, North Chelmsford, MA, Courier Corporation, 1981.

Jaffe, D., Anderson, T., Covert, D., Kotchenruther, R., Trost, B., Danielson, J., Simpson, W., Berntsen, T., Karlsdottir, S., Blake, D., Harris, J., Carmichael, G., and Uno, I.: Transport of Asian air pollution to North America, Geophysical Research Letters, 26(6), 711-714, https://doi.org/10.1029/1999GL900100, 1999.

Zhang, K., and Gao, H.: The characteristics of Asian-dust storms during 2000-2002: From the source to the sea, Atmospheric Environment, 41(39), 9136-9145, doi:10.1016/j.atmosenv.2007.08.007, 2007.

Liu, J., Yang, P., and Muinonen, K.: Dust-aerosol optical modeling with Gaussian spheres: Combined invariant-imbedding T-matrix and geometric-optics approach, Journal of Quantitative Spectroscopy and Radiative Transfer, 161, 136-144, http://dx.doi.org/10.1016/j.jqsrt.2015.04.003, 2015.

Liu, J., Zhang, Y., and Zhang, Q.: Laboratory measurements of light scattering matrices for resuspended small loess dust particles at 532 nm wavelength, Journal of Quantitative Spectroscopy and Radiative Transfer, 229,71-79, https://doi.org/10.1016/j.jqsrt.2019.03.010, 2019.

Liu, J., Zhang, Y., Zhang, Q., and Wang, J.: Scattering Matrix for Typical Urban Anthropogenic Origin Cement Dust and Discrimination of Representative Atmospheric Particulates, Journal of Geophysical Research: Atmospheres, 123(6), 3159-3174, https://doi.org/10.1002/2018JD028288, 2018.

Liu, L., Mishchenko, M. I., Hovenier, J. W., Volten, H., and Muñoz, O.: Scattering matrix of quartz aerosols: comparison and synthesis of laboratory and Lorenz–Mie results, Journal of Quantitative Spectroscopy and Radiative Transfer, 79, 911-920, https://doi.org/10.1016/S0022-4073(02)00328-X, 2003.

Merikallio, S., Muñoz, O., Sundström, A. M., Virtanen, T. H., Horttanainen, M., Leeuw, G. d., and Nousiainen, T.: Optical modeling of volcanic ash particles using ellipsoids, Journal of Geophysical Research: Atmospheres, 120(9), 4102-4116, https://doi.org/10.1002/2014JD022792, 2015.

Miffre, A., Mehri, T., Francis, M., and Rairoux, P.: UV-VIS depolarization from Arizona Test Dust particles at exact backscattering angle, Journal of Quantitative Spectroscopy and Radiative Transfer, 169, 79-90, https://doi.org/10.1016/j.jqsrt.2015.09.016, 2016.

Mishchenko, M., and Hovenier, J.: Depolarization of light backscattered by randomly oriented nonspherical particles, Optics Letters, 20(12), 1356-1358, https://doi.org/10.1364/OL.20.001356, 1995.

Mishchenko, M. I., Travis, L. D., and Lacis, A. A.: Scattering, absorption, and emission of light by small particles, Cambridge, UK: Cambridge University press, 2002.

Mishchenko, M. I., and Yurkin, M. A.: On the concept of random orientation in far-field electromagnetic scattering by nonspherical particles, Optics letters, 42(3), 494-497, https://doi.org/10.1364/OL.42.000494, 2017.

Mokhtari, T., Sorensen, C. M., and Chakrabarti, A.: Multiple-scattering effects on static light-scattering optical structure factor measurements, Applied optics, 44(36), 7858-7861, https://doi.org/10.1364/AO.44.007858, 2005.

Muñoz, O., and Hovenier, J.: Laboratory measurements of single light scattering by ensembles of randomly oriented small irregular particles in air. A review, Journal of Quantitative Spectroscopy and Radiative Transfer, 112(11), 1646-1657, https://doi.org/10.1016/j.jqsrt.2011.02.005, 2011.

Muñoz, O., Moreno, F., Guirado, D., Dabrowska, D., Volten, H., and Hovenier, J.: The Amsterdam–Granada light scattering database, Journal of Quantitative Spectroscopy and Radiative Transfer, 113(7), 565-574, https://doi.org/10.1016/j.jqsrt.2012.01.014, 2012.

Muñoz, O., Moreno, F., Guirado, D., Ramos, J., López, A., Girela, F., Jerónimo, J., Costillo, L., and Bustamante, I.: Experimental determination of scattering matrices of dust particles at visible wavelengths: The IAA light scattering

apparatus, Journal of Quantitative Spectroscopy and Radiative Transfer, 111(1), 187-196, doi: 10.1016/j.jqsrt.20 09.0 6.011, 2010.

Muñoz, O., Volten, H., De Haan, J., Vassen, W., and Hovenier, J.: Experimental determination of scattering matrices of olivine and Allende meteorite particles, Astronomy and Astrophysics, 360, 777-788, 2000.

Muñoz, O., Volten, H., De Haan, J., Vassen, W., and Hovenier, J.: Experimental determination of scattering matrices of randomly oriented fly ash and clay particles at 442 and 633 nm, Journal of Geophysical Research: Atmospheres, 106(D19), 22833-22844, https://doi.org/10.1029/2000JD000164, 2001.

Muñoz, O., Volten, H., Hovenier, J., Nousiainen, T., Muinonen, K., Guirado, D., Moreno, F., and Waters, L.: Scattering matrix of large Saharan dust particles: experiments and computations, Journal of Geophysical Research: Atmospheres, 112(D13), https://doi.org/10.1029/2006JD008074, 2007.

Muinonen, K., Zubko, E., Tyynelä, J., Shkuratov, Y. G., and Videen, G.: Light scattering by Gaussian random particles with discrete-dipole approximation, Journal of Quantitative Spectroscopy and Radiative Transfer, 106(1-3), 360-377, doi:10.1016/j.jqsrt.2007.01.049, 2007.

Satheesh, S., and Moorthy, K. K.: Radiative effects of natural aerosols: A review, Atmospheric Environment, 39(11), 2089-2110, https://doi.org/10.1016 /j.atmosenv.2004.12.029, 2005.

Shen, X., Sun, J., Zhang, Y., Zhang, X., Wang, T., Wang, Y., Zhang, L., Fan, R., Zhao, Y., and Wang, D, The influence of Asian dust outflow on particle microphysical and optical properties at Mt. Tai in central east China, Atmospheric Environment, 143, 27-38, http://dx.doi.org/10.1016/j.atmosenv.2016.08.014, 2016.

Sokolik, I. N., and Toon, O. B.: Direct radiative forcing by anthropogenic airborne mineral aerosols, Nature, 381(6584), 681, https://doi.org/10.1038/381681a0, 1996.

Tegen, I., and Fung, I.: Contribution to the atmospheric mineral aerosol load from land surface modification, Journal of Geophysical Research: Atmospheres, 100(D9), 18707-18726, https://doi.org/10.1029/95JD02051, 1995.

Tsai, F., Tu, J. Y., Hsu, S. C., and Chen, W. N.: Case study of the Asian dust and pollutant event in spring 2006: Source, transport, and contribution to Taiwan, Science of the Total Environment, 478, 163-174, http://dx.doi.org/10.1016/j.scitotenv.2014.01.072, 2014.

Volten, H., Muñoz, O., Hovenier, J., and Waters, L.: An update of the Amsterdam light scattering database, Journal of Quantitative Spectroscopy and Radiative Transfer, 100(1-3), 437-443, https://doi.org/10.1016/j.jqsrt.2005.11.055, 2006a.

Volten, H., Munoz, O., Brucato, J., Hovenier, J., Colangeli, L., Waters, L., and Van der Zande, W.: Scattering matrices and reflectance spectra of forsterite particles with different size distributions, Journal of Quantitative Spectroscopy and Radiative Transfer, 100(1-3), 429-436, https://doi.org/10.1016/j.jqsrt.2005.11.074, 2006b.

Volten, H., Munoz, O., Hovenier, J., de Haan, J., Vassen, W., Van der Zande, W., and Waters, L.: WWW scattering matrix database for small mineral particles at 441.6 and 632.8 nm, Journal of Quantitative Spectroscopy and Radiative Transfer, 90(2), 191-206, https://doi.org/10.1016/j.jqsrt.2004.03.011, 2005.

Volten, H., Munoz, O., Rol, E., Haan, J. d., Vassen, W., Hovenier, J., Muinonen, K., and Nousiainen, T.: Scattering matrices of mineral aerosol particles at 441.6 nm and 632.8 nm, Journal of Geophysical Research: Atmospheres, 106(D15), 17375-17401, https://doi.org/10.1029/2001JD900068, 2001.

Wang, Y., Chakrabarti, A., and Sorensen, C. M.: A light-scattering study of the scattering matrix elements of Arizona Road Dust, Journal of Quantitative Spectroscopy and Radiative Transfer, 163, 72-79, https://doi.org/10.1016/j.jqsrt.2015.05.002, 2015.

Xuan, J., Sokolik, I. N., Hao, J., Guo, F., Mao, H., and Yang, G.: Identification and characterization of sources of atmospheric mineral dust in East Asia, Atmospheric Environment, 38(36), 6239-6252, https://doi.org/10.1016/j.atmosenv.2004.06.042, 2004.

Yan, Y., Sun, Y., Ma, L., and Long, X.: A multidisciplinary approach to trace Asian dust storms from source to sink, Atmospheric Environment, 105, 43-52, http://dx.doi.org/10.1016/j.atmosenv.2015.01.039, 2015.

Zhang, K., Chai, F., Zhang, R., and Xue, Z.: Source, route and effect of Asian sand dust on environment and the oceans, Particuology, 8(4), 319-324, doi:10.1016/j.partic.2010.03.016, 2010.

Zhang, X., Gong, S., Shen, Z., Mei, F., Xi, X., Liu, L., Zhou, Z., Wang, D., Wang, Y., and Cheng, Y.: Characterization of soil dust aerosol in China and its transport and distribution during 2001 ACE-Asia: 1. Network observations, Journal of Geophysical Research: Atmospheres, 108(D9), doi:10.1029/2002JD002632, 2003.

Zubko, E., Muinonen, K., Muñoz, O., Nousiainen, T., Shkuratov, Y., Sun, W., and Videen, G.: Light scattering by feldspar particles: comparison of model agglomerate debris particles with laboratory samples, Journal of Quantitative Spectroscopy and Radiative Transfer, 131, 175-187, https://doi.org/10.1016/j.jqsrt.2013.01.017, 2013.

Zubko, E., Muinonen, K., Shkuratov, Y., Videen, G., and Nousiainen, T.: Scattering of light by roughened Gaussian random particles, Journal of Quantitative Spectroscopy and Radiative Transfer, 106(1-3), 604-615, doi:10.1016/j.jqsrt.2007.01.050, 2007.

https://doi.org/10.5194/amt-2019-236
Preprint. Discussion started: 9 August 2019

Atmospheric Measurement Techniques Discussions

455

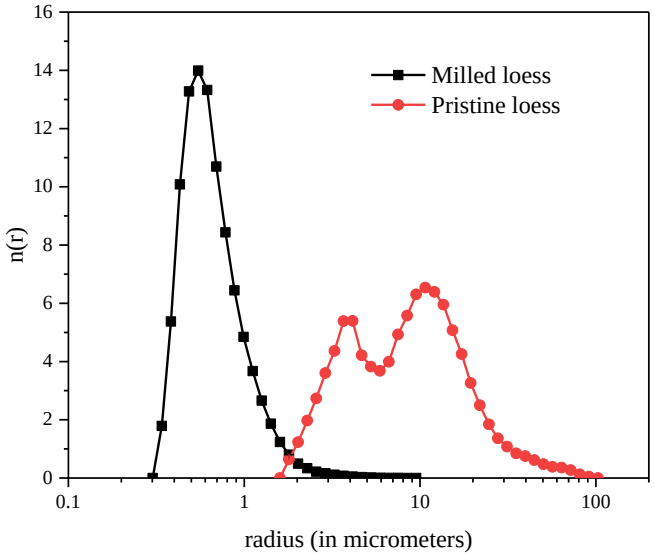

Figure 1. Normalized number distributions of "pristine loess" and "milled loess". Radius is plotted in logarithmic scale, and error bars are so small that are covered by symbols.

https://doi.org/10.5194/amt-2019-236
Preprint. Discussion started: 9 August 2019

Atmospheric Measurement Techniques Discussions

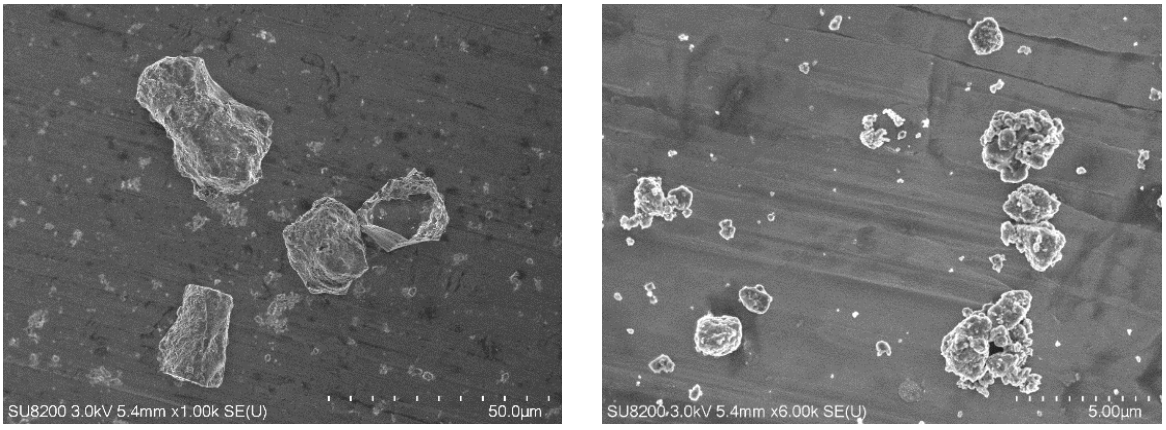

460

Figure 2. SEM images for “pristine loess” (left panel) and “milled loess” (right panel).

https://doi.org/10.5194/amt-2019-236
Preprint. Discussion started: 9 August 2019

Atmospheric Measurement Techniques Discussions

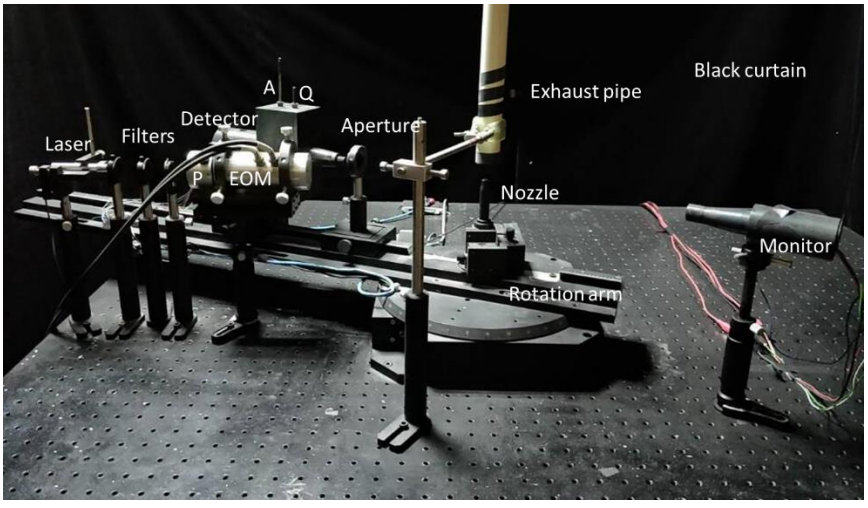

Figure 3. Photograph of the experimental apparatus. Rotation arm is fixed at 160 °angle.

465

https://doi.org/10.5194/amt-2019-236
Preprint. Discussion started: 9 August 2019

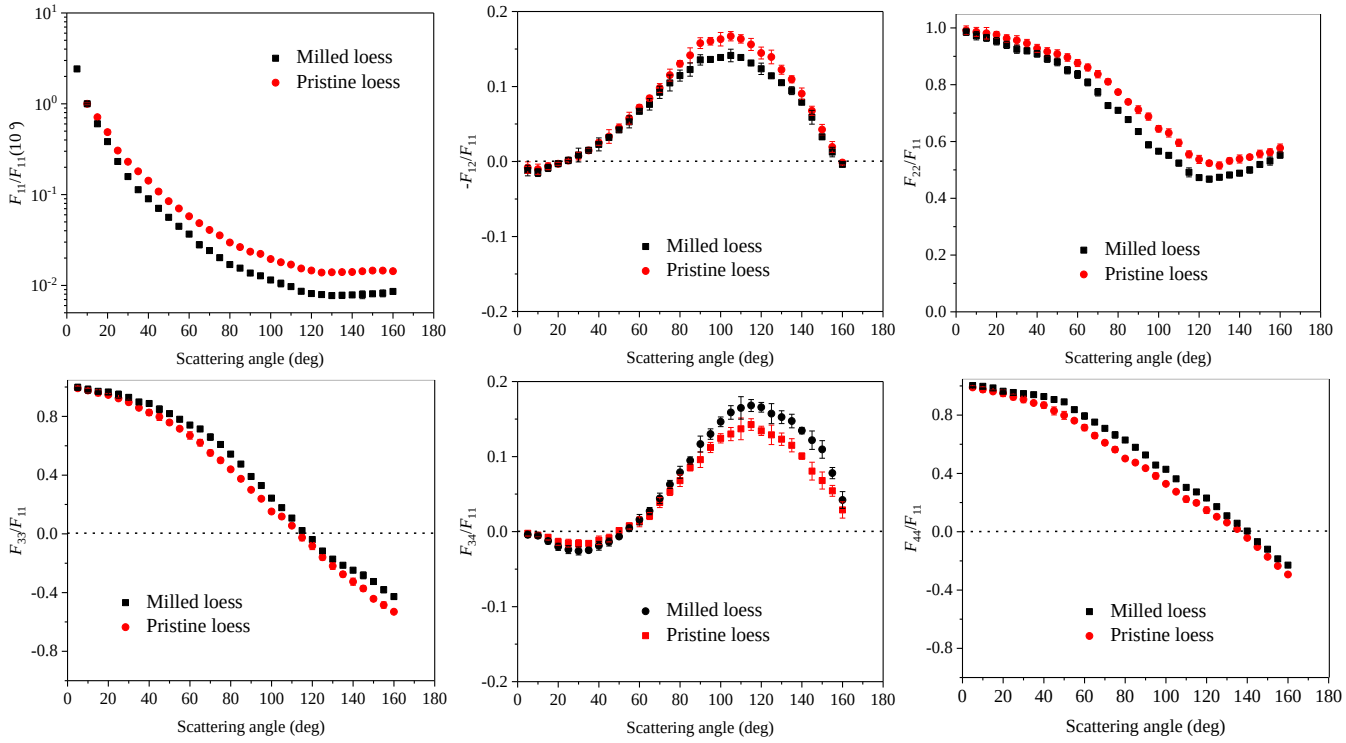

Figure 4. Measured non-zero scattering matrices for “pristine loess” and “milled loess”. It should be noted that "milled loess" is the same sample as the "Luochuan loess" in Liu et al. (2019).

https://doi.org/10.5194/amt-2019-236
Preprint. Discussion started: 9 August 2019

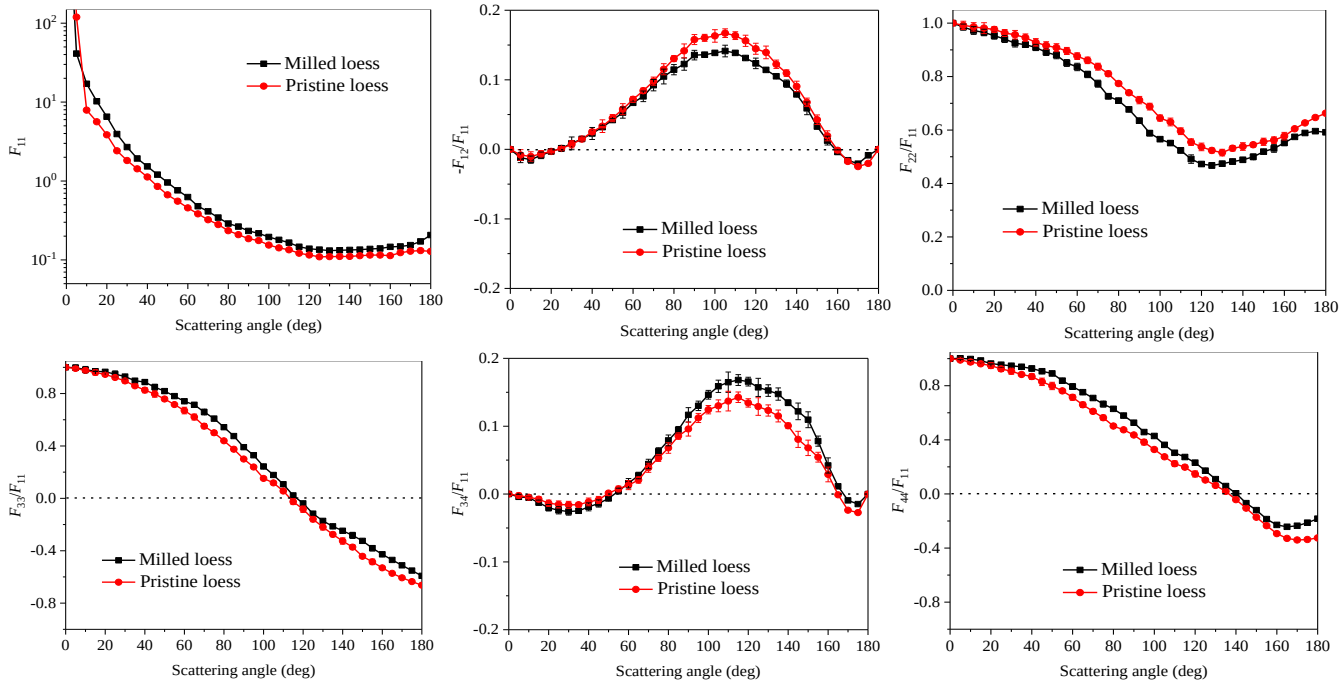

Figure 5. Synthetic scattering matrices for “milled loess” and “pristine loess” (Liu et al., 2019).

https://doi.org/10.5194/amt-2019-236
Preprint. Discussion started: 9 August 2019

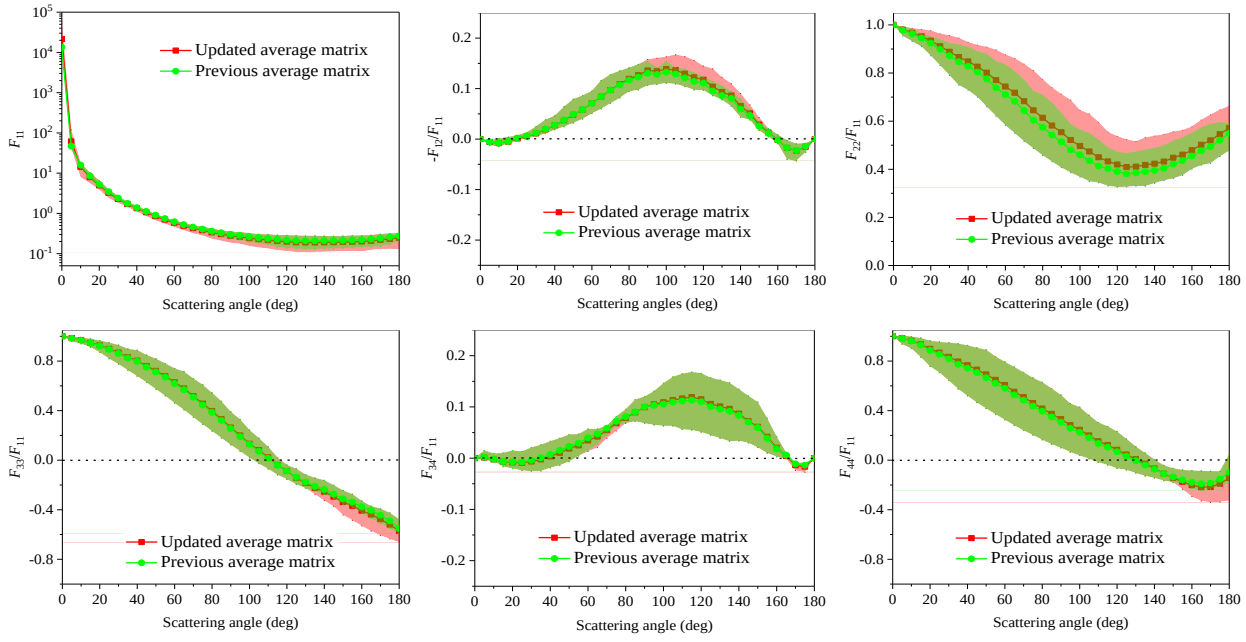

Figure 6. Previous average scattering matrix (red lines and solid squares) (Liu et al., 2019) and updated average scattering matrix (green lines and solid circles). Reddish domains and green domains stand for the areas covered by measurements of different loess samples with or without "pristine loess" included, respectively.

https://doi.org/10.5194/amt-2019-236
Preprint. Discussion started: 9 August 2019

Atmospheric Measurement Techniques Discussions

Table 1. Size parameters and refractive indices of "pristine loess" and "milled loess".

Samples	r_{eff} (μm)	σ_{eff}	x_{eff}	$Re(m)$	$Im(m)$
Pristine loess	49.40 ± 1.98	0.21 ± 0.00	583.2 ± 23.7	1.65	0
Milled loess	2.35 ± 0.01	0.64 ± 0.00	27.2 ± 0.1	1.70	0

480

https://doi.org/10.5194/amt-2019-236
Preprint. Discussion started: 9 August 2019

Atmospheric Measurement Techniques Discussions

Table 2. Chemical components of "pristine loess" and "milled loess".

Components	Pristine loess (wt %)	Milled loess (wt %)
SiO_2	65.9658	67.6906
Al_2O_3	12.0424	11.5060
CaO	8.6257	7.3725
Fe_2O_3	4.9025	5.1149
K_2O	3.1846	3.1906
MgO	2.4338	2.2958
Na_2O	1.2630	1.3318
TiO_2	0.7596	0.7529
P_2O_5	0.3020	0.2536
SO_3	0.3116	0.2197
MnO	0.1032	0.1111
ZrO_2	0.0509	0.0932
SrO	0.0303	0.0257
Co_2O_3	NT*	0.0193
Rb_2O	0.0148	0.0145
Y_2O_3	NT*	0.0078

* NT: not detected.